Structural Dynamics of the Actomyosin Complex Probed by a Bifunctional Spin Label that Cross-Links SH1 and SH2

Andrew R. Thompson,* Nariman Naber,† Clyde Wilson,† Roger Cooke,†‡ and David D. Thomas*
*Department of Biochemistry, Molecular Biology and Biophysics, University of Minnesota, Minneapolis, Minnesota; and †Department of Biochemistry and Biophysics and ‡Cardiovascular Research Institute, University of California, San Francisco, California

ABSTRACT We have used a bifunctional spin label (BSL) to cross-link Cys^{707} (SH1) and Cys^{697} (SH2) in the catalytic domain of myosin subfragment 1 (S1). BSL induces the same weakened ATPase activity and actin-binding affinity that is observed when SH1 and SH2 are cross-linked with pPDM, which traps an analog of the post-hydrolysis state A·M·ADP·P. Electron paramagnetic resonance showed that BSL reports the global orientation and dynamics of S1. When bound to actin in oriented muscle fibers in the absence of ATP, BSL-S1 showed almost complete orientational disorder, as reported previously for the weakly bound A·M·ADP. In contrast, helical order is observed for the strongly bound state A·M. Saturation transfer electron paramagnetic resonance showed that the disorder of cross-linked S1 on actin is nearly static on the microsecond timescale, at least 30 times slower than that of A·M·ADP. We conclude that cross-linked S1 exhibits rotational disorder comparable to that of A·M·ADP, slow rotational mobility comparable to that of A·M, and intermediate actin affinity. These results support the hypothesis that the catalytic domain of myosin is orientationally disordered on actin in a post-hydrolysis state in the early stages of force generation.

INTRODUCTION

Muscle contraction is produced when actin activates the hydrolysis of ATP by myosin, resulting in relative translation of the two proteins. Force generation has been proposed to originate from transition of the myosin catalytic domain (CD) from a disordered state of weak actin binding to an ordered state of strong actin binding, followed by a lever arm rotation of the light-chain domain (LCD) (1–3) (Fig. 1). The strongly bound complexes A·M and A·M·D have been studied in great detail. In the absence of nucleotide or in the presence of MgADP, actin and myosin interact such that the orientations of both the catalytic (4,5) and light-chain (6) domains are well defined with respect to the actin filament axis. However, much less is known about the structures of the weakly bound complexes (A·M·T and A·M·D·P), not only because of their dynamic disorder, but also because they are short-lived. Saturation transfer EPR (STEPR) in the steady state of ATP hydrolysis (7,8) or in the presence of ATPγS (9,10) has shown clearly that weakly attached myosin heads undergo large-amplitude rotational motions with correlation times in the range of 1–20 μs, consistent with the orientationally disordered appearance of subfragment 1 (S1) bound to actin in electron micrographs of similar weakly bound complexes (11–13).

However, all of these EPR and electron microscopy (EM) experiments were done under conditions in which the predominant actin-attached states were most likely the prehydrolysis complex A·M·T. The post-hydrolysis complex A·M·D·P is potentially of much more interest, since there is evidence that force generation begins in this biochemical state, before phosphate is released (14,15). This complex has remained elusive for two reasons: 1), actin greatly accelerates the release of P_i from myosin (converting A·M·D·P to A·M·D); and 2), actin shifts the equilibrium constant for hydrolysis toward the prehydrolysis state (converting A·M·D·P to A·M·T) by a factor of 20 (16). It has not proven feasible to prepare a stable complex of actin with myosin using the post-hydrolysis analogs ADP·V_i and ADP·AlF_4, because actin rapidly dissociates the phosphate analogs from the complex (17,18). The nucleotide analogs AMPPNP and pyrophosphate do remain bound in ternary complexes with actin and myosin, but these complexes are indistinguishable from the strongly bound complex A·M·D (9,19,20).

There is one relatively stable equilibrium complex, though, that has been proposed to have the biochemical and structural properties of the ternary complex A·M·D·P: the complex of actin with myosin S1 that has been reacted with pPDM, which specifically cross-links SH1 (Cys^{707}) to SH2 (Cys^{697}) (21–23). It was found that pPDM-S1 exhibits weak actin binding, with an actin affinity at low ionic strength (K_d = 30 μM) only ~3 times stronger than S1·ATP, 100 times weaker than S1·AMPPNP, and 1000 times weaker than S1·ADP (22). The observation that ADP-bound S1 has three orders of magnitude greater actin affinity seems surprising, considering that pPDM traps MgADP during cross-linking

Submitted May 30, 2008, and accepted for publication September 2, 2008.

Andrew R. Thompson. and Nariman Naber contributed equally to this work.

Address reprint requests to David D. Thomas. University of Minnesota Medical School, Dept. of Biochemistry, 6-155 Jackson Hall, 321 Church St. SE, Minneapolis, MN 55455. Tel.: 612-625-0957; E-mail: ddt@umn.edu.

Abbreviations: BSL, 3,4-bis-(methanethiosulfonyl-methyl)-2,2,5,5-tetramethyl-2,5-dihydro-1h-pyrrol-1-yloxy; pPDM, N,N′-(1,4-phenylene)dimaleimide; EPR, electron paramagnetic resonance; STEPR, saturation transfer electron paramagnetic resonance; IASL, 4-(2-iodoacetamido)-2,2,6,6-tetramethylpiperidine 1-oxyl; MTSSL, (1-oxy-2,2,5,5-tetramethyl-Δ^3-pyrroline-3-methyl) methanethiosulfonate.

Editor: Christopher Lewis Berger.

0006-3495/08/12/5238/09 $2.00

doi: 10.1529/biophysj.108.138982

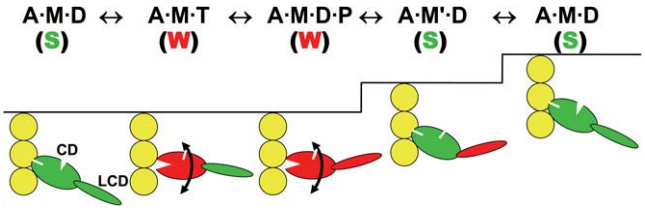

FIGURE 1 Structural model by which ATP hydrolysis is coupled to movement of actin (*yellow*) by myosin's CD and LCD. Red and green colors signify pre- and post-force-generating conformations, arrows signify orientational disorder, and steps indicate stages in the cycles where force and movement are likely to be imparted to actin. A = actin, M = myosin, T = ATP, D = ADP, P = inorganic phosphate, S = strong-binding (force-generating) structural state, and W = weak-binding structural state. The prime symbol (′) indicates a second structural state corresponding to the same biochemical state (defined by the active-site ligand).

and MgADP accelerates the reaction of pPDM with S1 (24,25). However, the removal of MgADP after pPDM cross-linking has little effect on the properties of pPDM-S1, so the weak binding is not a function of the trapped nucleotide (21). Chemical (25), spectroscopic (26), and crystallographic (27) analyses suggested a structural explanation: pPDM is much too short to cross-link Cys^{697} to Cys^{707} in the crystal structure of S1 (28), so nucleotide binding results in the disordering of the intervening SH1 helix, permitting the two Cys residues to approach, at least transiently, within the pPDM cross-linking distance. Therefore, it is likely that pPDM-S1 is a structural and functional analog for a weak-binding post-hydrolysis state A·M·D·P, and thus there is a need for spectroscopic data to characterize the structure and dynamics of this complex.

However, the reaction of pPDM blocks SH1 and SH2, thus preventing the use of the SH1-bound spin labels that have been so useful in characterizing the orientation and dynamics of myosin CDs bound to actin. To solve this problem, in the study presented here we used a bifunctional spin label (BSL) that is itself a cysteine cross-linker. We show that it binds rigidly and specifically to S1, cross-linking SH1 and SH2. To obtain information about the orientation of the spin-labeled S1 relative to actin, and to overcome the weak binding of the cross-linked S1 to actin, we performed EPR experiments in skinned muscle fibers, where the free actin concentration is ~360 μM (29). We decorated these fibers with spin-labeled S1 and then used both conventional and STEPR to determine the orientation and rotational dynamics of the actin-attached myosin heads in this weak-binding analog of A·M·D·P.

MATERIALS AND METHODS

Preparation of proteins and muscle fibers

Myosin, chymotryptic myosin S1, and actin were prepared from rabbit skeletal muscle as described previously (17). Concentrations were determined from UV absorbance: $[myosin] = (A^{280}–A^{320})/(2.49 \times 10^5\ M^{-1}cm^{-1})$, $[S1] = (A^{280}–A^{320})/(8.07 \times 10^4\ M^{-1}cm^{-1})$, $[actin] = (A^{290}–A^{320})/(2.71 \times 10^4\ M^{-1}cm^{-1})$. Glycerinated rabbit psoas muscle fiber strips (~2 mm diameter) were prepared and stored in a 1:1 (vol:vol) mixture of rigor buffer (120 mM KCl, 25 mM morpholinopropane sulfonic acid (MOPS), 2 mM $MgCl_2$, 1 mM EGTA, pH 7.0) and glycerol at −20°C for up to 6 months without significant loss of function (30). All preparations and experiments described below were carried out at 4°C.

Monofunctional labeling

SH1 (Cys^{707}) of the myosin S1 head was spin-labeled with the monofunctional probes IASL (Sigma-Aldrich, St. Louis, MO) or MTSSL (Toronto Research Chemicals, North York, ON) as follows: 20 μM S1 was incubated with 30 μM spin label at 4°C in monofunctional labeling buffer (50 mM MOPS, 50 mM KCl, pH 7.0) for 16 h for IASL or 2 h for MTSSL. The unbound spin label was removed by passing the labeled protein twice through a Pierce Zeba size-exclusion spin column (Thermo Fisher Scientific Inc., Rockford, IL), which was equilibrated with monofunctional labeling buffer. S1 was then concentrated and transferred to low salt buffer (LSB; 2 mM $MgCl_2$, 1 mM EGTA, 40 mM MOPS pH 7) using an Amicon Centricon membrane concentrator (Millipore, Billerica, MA). The resulting purified protein is termed IASL-S1 or MTSSL-S1. To prepare IASL-myosin, the same procedure was used, except that removal of unbound label and concentration were accomplished by sedimentation and resuspension of myosin filaments (31).

Bifunctional labeling

SH1 (Cys^{707}) and SH2 (Cys^{697}) were cross-linked using either BSL (Toronto Research Chemicals, North York, ON) or pPDM (Sigma-Aldrich, St. Louis, MO). To a solution of 20 μM S1 in cross-linking buffer (1 mM ADP, 2 mM $MgCl_2$, 100 mM KCl, 40 mM Tris, pH 7.8), 24 μM BSL or 30 μM pPDM was added from freshly prepared stock solutions in dimethylformamide, such that the final dimethylformamide concentration never exceeded 1%. After 1 h, the unreacted cross-linker was removed and the protein was concentrated as described above for monofunctional labeling. The unreacted and monofunctionally labeled S1 were removed by cosedimentation with actin in LSB. The resulting purified preparations are termed BSL-S1 and pPDM-S1, respectively. To prepare BSL-myosin, the same procedure was used, except that removal of unbound label was accomplished by sedimentation and resuspension of myosin filaments (31).

Biochemical assays

To assess Cys labeling of SH1 and SH2, the K/EDTA and Ca/K ATPase activities were measured at high ionic strength by measuring phosphate liberation after acid quench (32). The incubation buffer (25°C) contained 50 mM MOPS and 0.6M KCl, pH 7.5, and either 5 mM EDTA (K/EDTA ATPase) or 10 mM $CaCl_2$ (Ca/K ATPase). The activity was checked by ATPase assays both before and after the acquisition of spectra to ensure stability of the observed state. The equilibrium constant for dissociation of labeled S1 from actin (K_d) was measured in LSB by cosedimentation (33).

To assess the weak or strong mode by which S1 binds to actin, the quenching of pyrene-labeled actin was measured (34). Actin was labeled at Cys^{374} with pyrene iodoacetamide (Invitrogen, Carlsbad, CA) (17), and fluorescence was measured using a Varian Cary Eclipse fluorometer (Varian Inc., Palo Alto, CA), with excitation and emission at 350 nm and 409 nm, respectively. S1 or labeled S1 was then added in excess of actin. Strong binding of S1 to actin was noted by a quenching of pyrene fluorescence, whereas weak binding (e.g., in the presence of saturating ATP) produced no change from the basal pyrene fluorescence (34).

EPR spectroscopy

For EPR experiments on spin-labeled myosin or S1 in solution, samples were dialyzed into LSB, adjusted to a final concentration of 100 μM myosin

heads, and then placed into a flame-sealed glass capillary (50 μL Wiretrol, Drummond Scientific, Broomall, PA). For experiments on actin-bound S1, skinned muscle fiber strips were dissected into bundles of ~0.5 mm diameter. The fibers were then soaked in the spin-labeled S1 solution in LSB (either IASL-S1 or BSL-S1) at a concentration of 100 μM or higher. After at least 2 h the fibers were washed several times with LSB to remove any unbound S1.

S1-decorated muscle fiber bundles were cut into 0.5 cm lengths and aligned to be perpendicular to the long axis of a quartz tissue flat cell that contained a well of dimensions 0.5 × 1.0 × 0.05 cm (WG-806-Q, Wilmad-Labglass, Buena, NJ). Excess moisture was wicked away from the fibers with a Kimwipe (Kimberly-Clark, Neenah, WI) and a coverslip was placed over the sample well, sealed with vacuum grease to prevent sample dehydration. The flat cell assembly was then centered in the EPR cavity using Teflon collets and the fiber axis was manually oriented parallel or perpendicular to the external magnetic field. To obtain randomly oriented fibers for STEPR and other experiments, fibers were minced with a razor blade, and random orientation was verified by showing that the spectrum was insensitive to the flat cell's orientation in the magnetic field. STEPR experiments were performed with the flat cell plane perpendicular to the applied field.

EPR spectra were obtained at X-band (9.5 GHz) with either a Bruker (Billerica, MA) EMX or E500 spectrometer, using a TE102 (Bruker 4102ST) cavity. The sample temperature was maintained at 4°C by flowing cold N_2 gas through a nozzle attached to the optical port on the front of the cavity. The sweep width was 120 G (1024 points), sweep time was typically 40 s, and the center field value H_C was set proportionally to the microwave frequency ($H_C = \nu/2.803$ MHz/G, corresponding to a g value of 2.0027, the value of g_z for a typical nitroxide) so that all spectra were equivalently aligned.

Conventional (V_1) spectra were recorded at a microwave field amplitude of $H_1 = 0.14$ G, with modulation frequency $\nu_m = 100$ kHz (first harmonic), peak-to-peak modulation amplitude $H_m = 1$ G, modulation phase $\phi_m = 0°$ (maximum signal), and filter time constant τ_F = conversion time. STEPR (V_2') spectra were recorded essentially as described previously (35), with $H_1 = 0.25$ G, $\nu_m = 50$ kHz, $H_m = 5$ G, phase-sensitive detection at 100 kHz (second harmonic), $\phi_m = 90°$ (minimum signal at nonsaturating power), and τ_F = twice the conversion time (due to the higher H_m, this does not distort the spectrum, since the linewidths are greater). Typically, the signal/noise ratio per scan was lower for V_2' than for V_1, so the number of scans was increased; typical acquisition times were 5 min for V_1 and 30 min for V_2'.

For each different sample configuration, H_1 was determined from $H_1 = C P^{1/2} Q_0/Q$, where C was determined by calibration with a sample of known saturation properties (peroxylamine disulfonate (35)), Q_0 is the cavity quality factor (measured by the spectrometer) during the original calibration, and Q is the value measured for each experiment. P was adjusted to obtain the desired H_1 value. For the standard flat cell configuration, $C = 1.0$ G/W$^{1/2}$ and $Q_0 = 1200$, so P was set at 20 mW × Q/1200 for V_1 and 63 mW × Q/1200 for V_2'.

Conventional EPR spectra (V_1) of spin-labeled S1 attached to actin in oriented muscle fibers were analyzed to determine the orientational distribution of the nitroxide spin label relative to the muscle fiber axis, using computational simulation and least-squares minimization as described previously (4,36). Briefly, the spectrum of minced fibers or precipitated S1 was first fit to obtain the orientation-independent parameters, such as the effective values for the anisotropic T and g matrices, and the linewidths. Using these values, spectra of oriented fibers were then fit to the orientational distribution of the spin label relative to the fiber axis, as defined by the center (θ_0') and width ($\Delta\theta'$, full width at half maximum) of the presumed Gaussian orientational distribution.

STEPR spectra (V_2') of randomly oriented samples (in solution or minced fibers) were analyzed to determine the effective rotational correlation time τ_R by measuring the ratio of the features L'' and L for μs–ms motion or C' and C for submillisecond motion, as defined previously (35). The position of L'' was taken as an average of height above baseline of the data 5–10 G to the right of L. The measured ratios L''/L and C'/C were then used to determine the rotational correlation time by comparison to the data for a model system shown in Fig. 3 of (35).

Quantification of the extent of spin labeling (spin labels bound per S1) was done by digital analysis of EPR spectra (37). Briefly, the double integral of the V_1 spectrum of a known concentration of S1 (typically 100 μM) was obtained at sufficiently low power to avoid saturation (typically 1 mW). This value was then compared to the double integral of a sample of known spin label concentration at the same microwave power and H_1 value to obtain the number of spin labels per S1.

RESULTS

BSL cross-links SH1 and SH2

The K-ATPase and Ca-ATPase activities, in conjunction with spin counts, were used to assess the extent and specificity of SH1 and SH2 labeling (Table 1). In both cases of monofunctional labeling (with IASL and MTSSL), the K-ATPase is inhibited by >85% and Ca-ATPase activated by >90%, indicating an essentially complete reaction with SH1 but not SH2 (38). For both BSL-S1 and pPDM-S1, the K-ATPase is also strongly inhibited, indicating essentially complete reaction with SH1, but the Ca-ATPase is <10% of that observed for IASL-S1 and MTSSL-S1, implying that at least 90% of SH2 has also been labeled (39). The result of EPR-based quantitation of the spin-label concentration (see Materials and Methods) yields 0.94 ± 0.07 mol of BSL per mole of S1. We conclude that virtually every S1 has both SH1 and SH2 blocked by a single spin label, which must be cross-linking the two cysteines (see Supplementary Material, Data S1). Cosedimentation with actin showed that monofunctionally labeled S1 binds actin strongly ($K_d < 1$ μM), in agreement with previous results (9), whereas both cross-linked S1 species bind actin much more weakly ($K_d \approx 30$ μM) (Table 1). Similarly, monofunctionally labeled S1 strongly quenched the fluorescence of pyrene-labeled actin, whereas neither BSL-S1 nor pPDM-S1 caused significant quenching, even when added at concentrations comparable to K_d. These results confirm that monofunctionally labeled S1 binds strongly to actin, whereas BSL-S1 binds weakly and has the same effect on actin structure as pPDM-S1 or S1·ATP (34). We conclude that BSL completely and specifically cross-links SH1 and SH2, giving BSL-S1 the same weak actin-binding properties as pPDM-S1.

The conventional (V_1) EPR spectra of both IASL-S1 and BSL-S1 indicate that the nitroxide probes are strongly immobilized on the protein, with an outer splitting $2T_\parallel' = 69.5$ G

TABLE 1 The effect of labeling S1 on ATPase activity and actin binding

Sample	Relative K-ATPase	Relative Ca-ATPase	K_d
IASL-S1	11 ± 4	1080 ± 70	<1 μM
MTSSL-S1	13 ± 7	960 ± 90	<1 μM
BSL-S1	8 ± 6	79 ± 6	31 ± 6 μM
pPDM-S1	12 ± 9	45 ± 7	30 ± 7 μM

ATPase values are % (mean ± SE) of unmodified S1 values, 8.7 ± 0.5 s^{-1} (K-ATPase) and 0.92 ± 0.07 s^{-1} (Ca-ATPase).

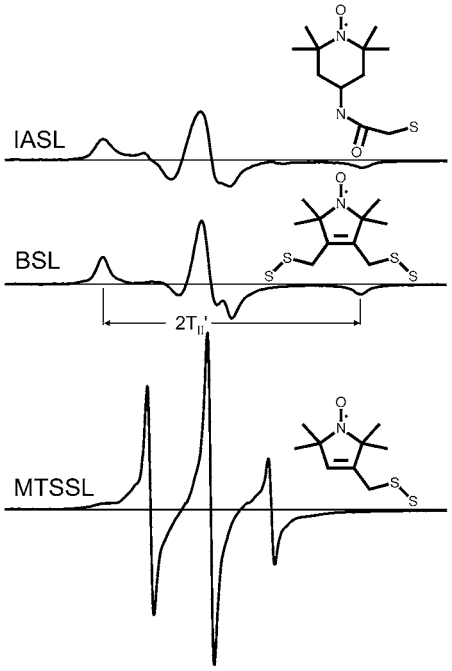

FIGURE 2 Conventional (V_1) EPR spectra of spin-labeled S1 (100 μM) in LSB at 4°C.

(Fig. 2) corresponding to that predicted for slow tumbling of S1 in solution, with a rotational correlation time of ~200 ns (40). In contrast, MTSSL, the monofunctional version of BSL, shows a narrow spectrum indicating a high degree of mobility in the subnanosecond time range (Fig. 2), despite its attachment to the same SH1 site as IASL. This result indicates that BSL's immobilization is due to bifunctional attachment to S1, at both SH1 and SH2, as indicated by Table 1.

EPR of oriented muscle fibers decorated with S1

EPR has a high degree of sensitivity to the orientational distribution of a spin label with respect to the externally applied magnetic field. The spectrum is sensitive primarily to the angle θ between the spin label's principal axis and the field. In a well-oriented system, such as skinned muscle fibers, this sensitivity can be used to measure the orientation of the probe with respect to the fiber axis (θ') (4), as simulated in Fig. 3. When the fibers are aligned on a flat cell, the fiber axis can be oriented either parallel (*red*, where $\theta = \theta'$) or perpendicular (*blue*, where θ' exhibits more disorder due to helical symmetry, as illustrated in Fig. 3) to the applied magnetic field.

The orientation of spin-labeled S1 bound to actin, with respect to the actin filament axis, was determined from EPR spectra of S1-decorated muscle fibers (Fig. 4). As shown previously, fibers decorated with IASL-S1 show a high degree of orientational order with respect to the fiber axis (Fig. 4, top), indicating that the angles (defined in Fig. 3) are $\theta' = 68 \pm 1°$ and $\Delta\theta' = 17 \pm 2°$ (4). In contrast, fibers decorated with BSL-S1 yield spectra that are characteristic of near random orientation ($\Delta\theta' \geq 90°$), having little sensitivity to sample orientation with respect to the applied magnetic field (Fig. 4, *bottom*). We conclude that BSL-S1, bound to oriented actin in the muscle fiber, shows a profound degree of orientational disorder relative to the actin filament axis. The next question is: Is this disorder dynamic on the microsecond timescale, as observed previously for S1 weakly bound to actin in a ternary complex with ATP (7), or static? This question can only be answered by STEPR.

STEPR

In addition to orientation, EPR is also sensitive to rotational dynamics on timescales of picoseconds to microseconds. To ensure that any observed spectral changes are due only to dynamics, samples must be randomly oriented. However, conventional (V_1) EPR is sensitive only to motions with rotational correlation times (τ_R) in the picosecond to nanosecond range (Fig. 5, *left*). For slower motions (microseconds to milliseconds), such as those likely to occur for a large protein or within a large protein assembly, STEPR must be used (Fig. 5, *right*) (35,42).

Conventional EPR (V_1) and STEPR (V_2') measurements were performed on randomly oriented samples of IASL-S1

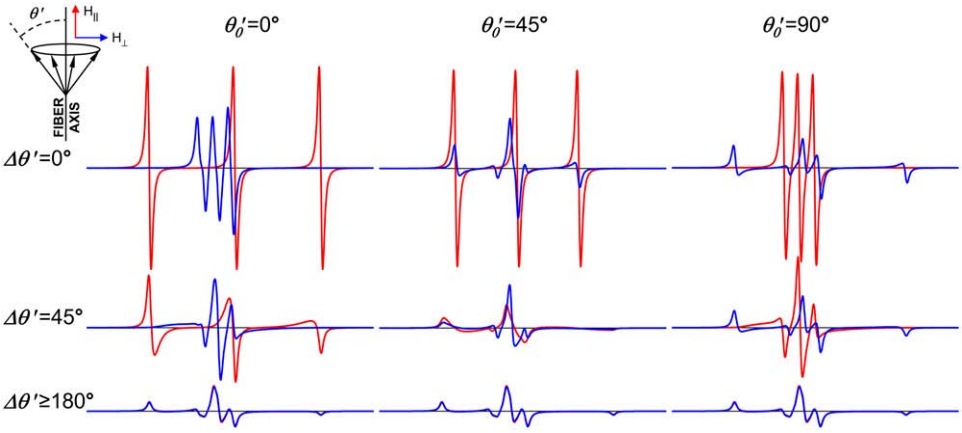

FIGURE 3 Simulated EPR spectra showing the dependence of conventional (V_1) EPR spectra on the orientation θ' of the nitroxide spin label's principal axis relative to the muscle fiber (actin filament) axis. A Gaussian distribution of θ' is assumed, where θ_0' is the center of the distribution and $\Delta\theta'$ is the full width at half-maximum. Spectra are shown corresponding to the muscle fiber axis both parallel (*red*) and perpendicular (*blue*) to the applied magnetic field (H).

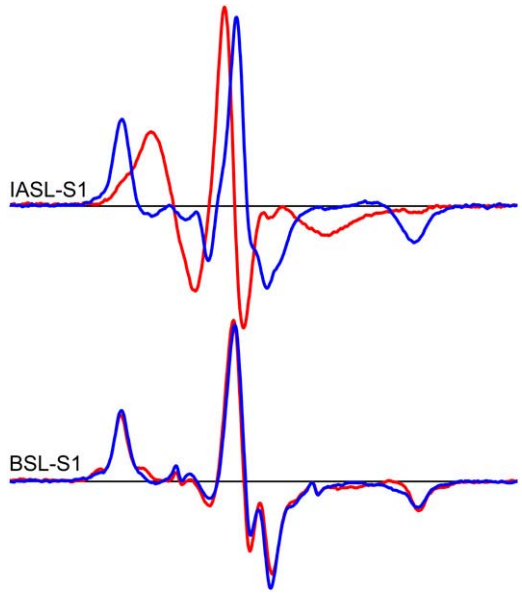

FIGURE 4 Oriented muscle fibers decorated with spin-labeled S1. The spectra were recorded with the fiber axis aligned parallel (*red*) or perpendicular (*blue*) to the external magnetic field in a quartz flat cell.

and BSL-S1 (Fig. 6) in a variety of environments, to determine the dynamics of the actin-bound CD. The conventional (V_1) spectra for both IASL-S1 and BSL-S1 have virtually no sensitivity to the different protein environments (Fig. 6), and all spectra have the characteristic ''powder'' shape, indicating that the rotational correlation time is >0.1 μs (Fig. 5). In contrast, STEPR (V_2') is quite sensitive to the changes in S1

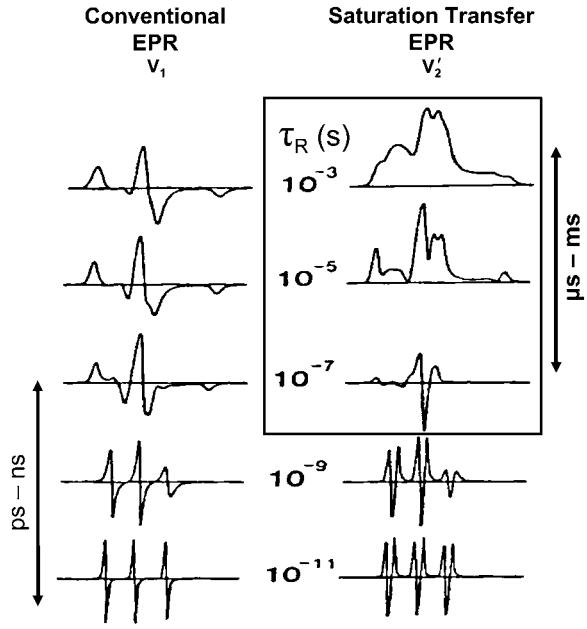

FIGURE 5 Dependence of conventional (V_1, *left*) and saturation transfer (V_2', *right*) EPR spectra on isotropic rotational correlation time (41).

environment (Fig. 6), demonstrating dynamics in the microsecond-to-millisecond time range (Fig. 5). Rotational correlation times for V_2' spectra were determined from line/height ratio parameters as described in Materials and Methods (35) (Table 2). We found that the rotational correlation times for BSL-S1 and IASL-S1 were identical within experimental error in all of the preparations studied (Table 2). The noticeable difference in V_2' lineshape between the two samples is due to the narrower intrinsic line width observed for BSL-S1, probably due to the more rigid coupling of the probe to the protein, which appears to affect small amplitude motions that have little effect on the V_2' lineshape parameters (43). For both spin labels, S1 free in solution (Fig. 6, *top row*) gave spectra characteristic of submicrosecond rotational motion (Table 2), as expected for the rigid-body tumbling of S1, whereas S1 precipitated in 20% polyethylene glycol (Fig. 6, *bottom row*) gave spectra approaching the rigid limit for STEPR, implying correlation times $\geq$1 ms (Table 2). Therefore, the microsecond rotational correlation times measured for other samples accurately reflect the global dynamics of the myosin head. Most importantly, the rotational correlation times for both IASL-S1 and BSL-S1 bound to actin (Fig. 6, *third row*) are both ~600 μs, nearly at the static limit for STEPR. This similarity in rotational correlation time is remarkable in light of the dramatic difference in the orientational distributions for these two spin labels (Fig. 4). The extremely slow motion is not surprising for IASL-S1, since this protein binds quite strongly to actin ($K_d < 1$ μM; Table 1). However, BSL-S1 binds much more weakly ($K_d = 30$ μM; Table 1) and has the same slow motion, despite previous reports that weak-binding myosin heads rotate on actin at least 30 times faster (7,44,45). This fast motion of weakly bound heads is simulated here for our probes by myosin filaments, which have a correlation time of 20 μs (Table 2), approximately the same as observed previously for S1 weakly bound to actin in a ternary complex with ATP (7,45). Thus BSL-S1 has the same orientational disorder on actin as observed for ATP-induced weak binding, but rotates 30 times more slowly.

DISCUSSION

Summary of results

When myosin S1 is reacted with a stoichiometric amount of BSL in the presence of ADP, a stable ternary complex is formed between the label, SH1, and SH2. Hi-salt ATPase activities (Table 1) and the EPR spectral intensity reveal that this reaction is highly specific and complete. Binding assays reveal that the affinity for actin (Table 1) is similar to that of the well-studied pPDM-S1 complex: BSL-S1 ($K_d = 30$ μM) binds much more weakly than S1 ($K_d < 1$ μM) but three times more strongly than S1·ATP ($K_d = 100$ μM at the same ionic strength (22)). The failure to quench pyrene-labeled actin fluorescence, even at concentrations exceeding K_d, confirms that the structural interactions in the acto-S1 com-

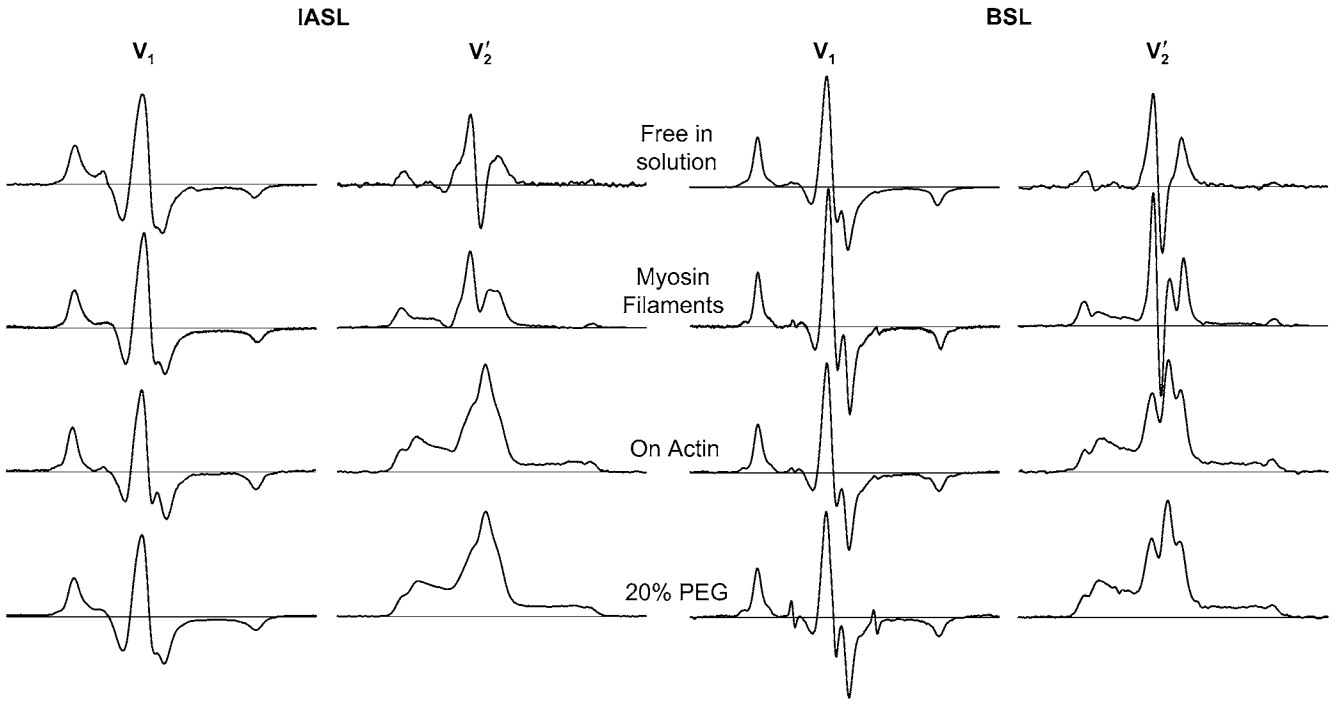

FIGURE 6 Conventional (V_1) and saturation transfer (V_2') EPR spectra for IASL-S1 (*left*) and BSL-S1 (*right*).

plex are of the same weak-binding nature as observed for pPDM. Consistent with the observed weak binding, EPR of BSL-S1 bound to actin reveals virtually complete orientational disorder relative to actin (Fig. 4), as observed previously for S1 in ternary complexes with actin and ATP (discussed below). This observation is in sharp contrast to the high degree of orientational order observed for the strongly bound IASL-S1. STEPR of these two preparations, on the other hand, reveals similar submillisecond rotational dynamics (Fig. 6), 30 times slower than observed for the ternary complex A·M·T, as modeled by A·M·ATPγS (Table 2) (9).

Interpretation of results

During the actomyosin ATPase cycle, myosin undergoes a weak-to-strong binding transition, accompanied by ATP hydrolysis and P_i release, in which the CD undergoes a disorder-to-order transition at the actin interface and the LCD rotates as a lever arm (Fig. 1). This two-step structural transition is proposed to generate force in muscle contraction (1–3). The weak-binding state, simulated here by myosin filaments (Fig. 6, *second row*), exhibits a high degree of orientational disorder on the microsecond timescale, similar to that of the A·M·T state measured directly (9,44). The strong-binding state, represented by IASL-S1, makes a bond to actin with a high degree of orientational order (Fig. 4, *top*) and at least 30-fold slower motion than A·M·T (Table 2). BSL-S1 exhibits characteristics of each: its motion is as slow ($\tau_R = 600\ \mu s$) as in the strong-binding state ($\tau_R = 560\ \mu s$, Table 2), but its orientation on actin is as poorly defined as in the weak-binding state (Fig. 4). These properties are accompanied by an affinity for actin that is also intermediate between the weak-binding and strong-binding states, as in the case of pPDM-S1 (Table 1). What biochemical intermediate might be trapped by the BSL cross-linker? To increase the specificity of BSL for SH1 and SH2 cross-linking, the reaction was done in the presence of MgADP, stoichiometrically trapping the nucleotide upon cross-linking. It would be natural, then, to conclude that we have trapped a state toward the end of the power stroke. This conclusion is greatly weakened, though, by the observations that the S1·ADP state binds actin 1000 times more strongly than does cross-linked S1 (22), and that removal of the bound ADP only slightly affects actin affinity (21). Therefore, we conclude that the SH1-SH2 helix is always in equilibrium between cross-linkable (disordered) and uncross-linkable (ordered) conformational states, and the nucleotide simply shifts the equilibrium between these

TABLE 2 Effective rotational correlation times (τ_R) from V_2' spectra (Fig. 6)

Sample	L″/L	C′/C	τ_R (μs)
IASL-S1		−0.26 ± 0.01	≤0.50
IASL-myosin	0.47 ± 0.01		18 ± 1
MSL-S1 on actin + ATPγS(9)	0.54 ± 0.05		24 ± 5
IASL-S1 on actin	1.44 ± 0.02		560 ± 40
IASL-S1 in 20% PEG	1.58 ± 0.02		≥1000
BSL-S1		0.18 ± 0.01	≤0.50
BSL-myosin	0.51 ± 0.01		21 ± 1
BSL-S1 on actin	1.46 ± 0.01		600 ± 20
BSL-S1 in 20% PEG	1.60 ± 0.01		≥1000

Values are mean ± SE (n = 3-6).

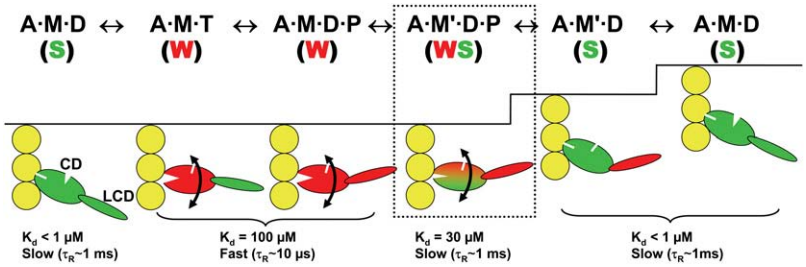

FIGURE 7 A revised model for the coupling of actomyosin ATP hydrolysis to force and movement, focusing on the coupling of biochemical transitions to structural dynamics of the myosin CD. The structural states and definitions are the same as in Fig. 1, except for the WS intermediate defined by this study. The text under each state indicates the distinguishing properties of the catalytic domain. The prime symbol (′) indicates a second structural state corresponding to the same biochemical state (defined by the active-site ligand). Although this scheme shows that structural transitions in the catalytic domain are completed before rotation of the LCD, this is probably an unnecessary assumption.

two states and thus the rate of cross-linking. Indeed, it has been shown that oPDM (*N*,*N*′-1,2-phenylene dimaleimide), a cross-linker of similar dimensions to BSL, reacts with SH1-SH2 at least four times faster in the presence of a post-hydrolysis analog ($ADPV_i$ or $ADPAlF_4$) than a prehydrolysis analog (46). This suggests that BSL cross-linking traps S1 in a state that mimics a post-hydrolysis ternary complex, A·M·D·P. This represents an important breakthrough, since this complex is proposed to initiate force generation (14,15) but is virtually impossible to trap in solution in the absence of cross-linking, as discussed in the Introduction.

Relationship to previous results

Our observation of slow orientational disorder of cross-linked S1 is consistent with previous studies. EM of pPDM-S1 bound to actin via a zero-length cross-linker reveals a high degree of orientational disorder (47), in stark contrast to the highly ordered arrowhead-shaped rigor acto-S1 complex (48). This level of orientational disorder is quite similar to that observed by EM when S1 is bound to actin in the presence of saturating ATP (11–13), and to the dynamic orientational disorder observed by EPR for actin-bound S1 in the presence of ATP (7,44) or ATPγS ((9), Table 2). Even in intact muscle fibers, myosin heads bound to actin and ATP, in the absence of calcium, show similar dynamic disorder of the CD (49). However, EPR of spin-labeled muscle fibers in the presence of aluminum fluoride and calcium revealed a state similar to that observed in this study for BSL-S1 (a slow disorder of the CD), leading the authors to suggest that this represents an intermediate state between weak binding and force generation (50). Together, these results suggest that the myosin CD enters the powerstroke when its dynamic (microsecond) disorder becomes much slower.

Alternative explanations

It is conceivable that the observed orientational disorder of BSL-S1 is due to internal disorder within S1 rather than global disorder of S1 due to weakening of the actomyosin interface. However, even if the SH1-SH2 helix unfolds, it seems unlikely that the orientational disorder would be as complete as we observed ($\Delta\theta' \geq 90°$, Figs. 3 and 4) while also being so slow. Note that the STEPR spectra are not consistent with more rapid (i.e., submicrosecond) motions that are more restricted, since STEPR measures the correlation time directly and accurately in the time domain from 0.1 to 1 ms (43). Furthermore, it is difficult to discount the orientational disorder observed in EM, as discussed above. Finally, it is not possible that the disorder is due to a significant population of dissociated heads, since the dissociation constant (30 μM; Table 1) is ~10 times less than the concentration of unoccupied actin (29).

Relationship to the mechanism of force generation

Our biochemical and EPR data indicate that we have trapped an intermediate state of the CD along the pathway from weak-binding disorder (W) to strong-binding order (S). In this new state, shown as A·M′·D·P (WS) in the revised scheme (Fig. 7), the myosin CD shares the orientational disorder of weak binding (*red*) and the slow dynamics of strong binding (*green*). The nucleotide-binding cleft is also beginning to open, as evidenced by the ability to freely exchange the trapped nucleotide with other nucleotides when on actin (21), providing the impetus for product release and the generation of mechanical force. We propose that the relatively slow rotational dynamics of this state compared to the truly weak-binding states A·M·T and A·M·D·P confers enough mechanical stability at the actomyosin interface to begin generating (and bearing) force. This model is consistent with mechanical evidence, both in muscle fibers and in isolated actomyosin, that the A·M′·D·P state initiates force generation (14,15).

SUPPLEMENTARY MATERIAL

To view all of the supplemental files associated with this article, visit www.biophysj.org.

This work was supported by National Institutes of Health (NIH) grants AR032961 (D.D.T.) and AR42895 (R.C.). A.R.T. was supported by National

Institute of Arthritis and Musculoskeletal and Skin Diseases/NIH training grant AR007612. We thank Leanne Kolb, Christina Yi, Sarah Blakely, and Octavian Cornea for excellent technical support; Yuri Nesmelov, Roman Agafonov, Ryan Mello, Jenny Klein, Ewa Prochniewicz, and Jack Surek for insightful discussions; and Edmund Howard for EPR analysis software.

REFERENCES

1. Thomas, D. D., S. Ramachandran, O. Roopnarine, D. W. Hayden, and E. M. Ostap. 1995. The mechanism of force generation in myosin: a disorder-to-order transition, coupled to internal structural changes. *Biophys. J.* 68:135S–141S.
2. Taylor, K. A., H. Schmitz, M. C. Reedy, Y. E. Goldman, C. Franzini-Armstrong, H. Sasaki, R. T. Tregear, K. Poole, C. Lucaveche, R. J. Edwards, L. F. Chen, H. Winkler, and M. K. Reedy. 1999. Tomographic 3D reconstruction of quick-frozen, Ca^{2+}-activated contracting insect flight muscle. *Cell.* 99:421–431.
3. LaConte, L. E., J. E. Baker, and D. D. Thomas. 2003. Transient kinetics and mechanics of myosin's force-generating rotation in muscle: resolution of millisecond rotational transitions in the spin-labeled myosin light-chain domain. *Biochemistry.* 42:9797–9803.
4. Thomas, D. D., and R. Cooke. 1980. Orientation of spin-labeled myosin heads in glycerinated muscle fibers. *Biophys. J.* 32:891–906.
5. Cooke, R., M. S. Crowder, and D. D. Thomas. 1982. Orientation of spin labels attached to cross-bridges in contracting muscle fibres. *Nature.* 300:776–778.
6. Baker, J. E., I. Brust-Mascher, S. Ramachandran, L. E. LaConte, and D. D. Thomas. 1998. A large and distinct rotation of the myosin light chain domain occurs upon muscle contraction. *Proc. Natl. Acad. Sci. USA.* 95:2944–2949.
7. Berger, C. L., E. C. Svensson, and D. D. Thomas. 1989. Photolysis of a photolabile precursor of ATP (caged ATP) induces microsecond rotational motions of myosin heads bound to actin. *Proc. Natl. Acad. Sci. USA.* 86:8753–8757.
8. Berger, C. L., and D. D. Thomas. 1993. Rotational dynamics of actin-bound myosin heads in active myofibrils. *Biochemistry.* 32:3812–3821.
9. Berger, C. L., and D. D. Thomas. 1991. Rotational dynamics of actin-bound intermediates in the myosin ATPase cycle. *Biochemistry.* 30: 11036–11045.
10. Berger, C. L., and D. D. Thomas. 1994. Rotational dynamics of actin-bound intermediates of the myosin adenosine triphosphatase cycle in myofibrils. *Biophys. J.* 67:250–261.
11. Craig, R., L. E. Greene, and E. Eisenberg. 1985. Structure of the actin-myosin complex in the presence of ATP. *Proc. Natl. Acad. Sci. USA.* 82:3247–3251.
12. Walker, M., J. Trinick, and H. White. 1995. Millisecond time resolution electron cryo-microscopy of the M-ATP transient kinetic state of the acto-myosin ATPase. *Biophys. J.* 68:87S–91S.
13. Walker, M., H. White, B. Belknap, and J. Trinick. 1994. Electron cryomicroscopy of acto-myosin-S1 during steady-state ATP hydrolysis. *Biophys. J.* 66:1563–1572.
14. Takagi, Y., H. Shuman, and Y. E. Goldman. 2004. Coupling between phosphate release and force generation in muscle actomyosin. *Philos. Trans. R. Soc. Lond. B Biol. Sci.* 359:1913–1920.
15. Smith, D. A., and J. Sleep. 2004. Mechanokinetics of rapid tension recovery in muscle: the myosin working stroke is followed by a slower release of phosphate. *Biophys. J.* 87:442–456.
16. White, H. D., B. Belknap, and M. R. Webb. 1997. Kinetics of nucleoside triphosphate cleavage and phosphate release steps by associated rabbit skeletal actomyosin, measured using a novel fluorescent probe for phosphate. *Biochemistry.* 36:11828–11836.
17. Prochniewicz, E., T. F. Walseth, and D. D. Thomas. 2004. Structural dynamics of actin during active interaction with myosin: different effects of weakly and strongly bound myosin heads. *Biochemistry.* 43:10642–10652.
18. Werber, M. M., Y. M. Peyser, and A. Muhlrad. 1992. Characterization of stable beryllium fluoride, aluminum fluoride, and vanadate containing myosin subfragment 1-nucleotide complexes. *Biochemistry.* 31: 7190–7197.
19. Pate, E., and R. Cooke. 1988. Energetics of the actomyosin bond in the filament array of muscle fibers. *Biophys. J.* 53:561–573.
20. Fajer, P. G., E. A. Fajer, N. J. Brunsvold, and D. D. Thomas. 1988. Effects of AMPPNP on the orientation and rotational dynamics of spin-labeled muscle cross-bridges. *Biophys. J.* 53:513–524.
21. Greene, L., J. Chalovich, and E. Eisenberg. 1986. Effect of nucleotide on the binding of N,N'-p-phenylenedimaleimide-modified S-1 to unregulated and regulated actin. *Biochemistry.* 25:704–709.
22. Chalovich, J., L. Greene, and E. Eisenberg. 1983. Cross-linked myosin subfragment 1: a stable analogue of the subfragment-1.ATP complex. *Proc. Natl. Acad. Sci. USA.* 80:4909–4913.
23. Bobkov, A., and E. Reisler. 2000. Is SH1–SH2-cross-linked myosin subfragment 1 a structural analog of the weakly-bound state of myosin? *Biophys. J.* 79:460–467.
24. Wells, J., and R. Yount. 1979. Active site trapping of nucleotides by cross-linking two sulfhydryls in myosin subfragment 1. *Proc. Natl. Acad. Sci. USA.* 76:4966–4970.
25. Burke, M., and E. Reisler. 1977. Effect of nucleotide binding on the proximity of the essential sulfhydryl groups of myosin. Chemical probing of movement of residues during conformational transitions. *Biochemistry.* 16:5559–5563.
26. Dalbey, R., J. Weiel, and R. Yount. 1983. Förster energy transfer measurements of thiol 1 to thiol 2 distances in myosin subfragment 1. *Biochemistry.* 22:4696–4706.
27. Houdusse, A., V. Kalabokis, D. Himmel, A. Szent-Gyorgyi, and C. Cohen. 1999. Atomic structure of scallop myosin subfragment S1 complexed with MgADP: a novel conformation of the myosin head. *Cell.* 97:459–470.
28. Rayment, I., W. R. Rypniewski, K. Schmidt-Base, R. Smith, D. R. Tomchick, M. M. Benning, D. A. Winkelmann, G. Wesenberg, and H. M. Holden. 1993. Three-dimensional structure of myosin subfragment-1: a molecular motor. *Science.* 261:50–58.
29. Bagshaw, C. R. 1993. Muscle Contraction. Chapman & Hall, New York. 155.
30. Prochniewicz, E., D. A. Lowe, D. J. Spakowicz, L. Higgins, K. O'Conor, L. V. Thompson, D. A. Ferrington, and D. D. Thomas. 2008. Functional, structural, and chemical changes in myosin associated with hydrogen peroxide treatment of skeletal muscle fibers. *Am. J. Physiol. Cell Physiol.* 294:C613–C626.
31. Barnett, V. A., and D. D. Thomas. 1987. Resolution of conformational states of spin-labeled myosin during steady-state ATP hydrolysis. *Biochemistry.* 26:314–323.
32. Lanzetta, P. A., L. J. Alvarez, P. S. Reinach, and O. A. Candia. 1979. An improved assay for nanomole amounts of inorganic phosphate. *Anal. Biochem.* 100:95–97.
33. Prochniewicz, E., and D. D. Thomas. 2001. Site-specific mutations in the myosin binding sites of actin affect structural transitions that control myosin binding. *Biochemistry.* 40:13933–13940.
34. Geeves, M. A., T. E. Jeffries, and N. C. Millar. 1986. ATP-induced dissociation of rabbit skeletal actomyosin subfragment 1. Characterization of an isomerization of the ternary acto-S1-ATP complex. *Biochemistry.* 25:8454–8458.
35. Squier, T. C., and D. D. Thomas. 1986. Methodology for increased precision in saturation transfer electron paramagnetic resonance studies of rotational dynamics. *Biophys. J.* 49:921–935.
36. Fajer, P. G., R. L. H. Bennett, C. F. Polnaszek, E. A. Fajer, and D. D. Thomas. 1990. General method for multiparameter fitting of high-resolution EPR spectra using a simplex algorithm. *J. Magn. Reson.* 88: 111–125.
37. Karim, C. B., Z. Zhang, and D. D. Thomas. 2007. Synthesis of TOAC spin-labeled proteins and reconstitution in lipid membranes. *Nat. Protocols.* 2:42–49.
38. Sekine, T., and W. W. Kielley. 1964. The enzymic properties of N-ethylmaleimide modified myosin. *Biochim. Biophys. Acta.* 81:336–345.

39. Reisler, E., M. Burke, and W. Harrington. 1974. Cooperative role of two sulfhydryl groups in myosin adenosine triphosphatase. *Biochemistry*. 13:2014–2022.

40. Thomas, D. D., J. C. Seidel, J. S. Hyde, and J. Gergely. 1975. Motion of subfragment-1 in myosin and its supramolecular complexes: saturation transfer electron paramagnetic resonance. *Proc. Natl. Acad. Sci. USA*. 72:1729–1733.

41. Thomas, D. D. 1977. Saturation transfer EPR. *Trends Biochem. Sci.* 2:N62–N63.

42. Thomas, D. D., L. R. Dalton, and J. S. Hyde. 1976. Rotational diffusion studied by passage saturation transfer electron paramagnetic resonance. *J. Chem. Phys.* 65:3006–3024.

43. Howard, E. C., K. M. Lindahl, C. F. Polnaszek, and D. D. Thomas. 1993. Simulation of saturation transfer electron paramagnetic resonance spectra for rotational motion with restricted angular amplitude. *Biophys. J.* 64:581–593.

44. Svensson, E. C., and D. D. Thomas. 1986. ATP induces microsecond rotational motions of myosin heads cross-linked to actin. *Biophys. J.* 50:999–1002.

45. Barnett, V. A., and D. D. Thomas. 1989. Microsecond rotational motion of spin-labeled myosin heads during isometric muscle contraction. Saturation transfer electron paramagnetic resonance. *Biophys. J.* 56:517–523.

46. Nitao, L. K., T. O. Yeates, and E. Reisler. 2002. Conformational dynamics of the SH1–SH2 helix in the transition states of myosin subfragment-1. *Biophys. J.* 83:2733–2741.

47. Flicker, P. F., R. A. Milligan, and D. Applegate. 1991. Cryo-electron microscopy of S1-decorated actin filaments. *Adv. Biophys.* 27:185–196.

48. Moore, P. B., H. E. Huxley, and D. J. DeRosier. 1970. Three-dimensional reconstruction of F-actin, thin filaments and decorated thin filaments. *J. Mol. Biol.* 50:279–295.

49. Fajer, P. G., E. A. Fajer, M. Schoenberg, and D. D. Thomas. 1991. Orientational disorder and motion of weakly attached cross-bridges. *Biophys. J.* 60:642–649.

50. Raucher, D., and P. G. Fajer. 1994. Orientation and dynamics of myosin heads in aluminum fluoride induced pre-power stroke states: an EPR study. *Biochemistry*. 33:11993–11999.